

Video Killed the HD-Map: Predicting Driving Behavior Directly From Drone Images

Yunpeng Liu^{1,2} Vasileios Lioutas^{1,2} Jonathan Wilder Lavington^{1,2} Matthew Niedoba^{1,2} Justice Sefas^{1,2}
Setareh Dabiri¹ Dylan Green^{1,2} Xiaoxuan Liang^{1,2} Berend Zwartsenberg¹ Adam Ścibior¹ Frank Wood^{1,2,3}*

Abstract

The development of algorithms that learn behavioral driving models using human demonstrations has led to increasingly realistic simulations. In general, such models learn to jointly predict trajectories for all controlled agents by exploiting road context information such as drivable lanes obtained from manually annotated high-definition (HD) maps. Recent studies show that these models can greatly benefit from increasing the amount of human data available for training. However, the manual annotation of HD maps which is necessary for every new location puts a bottleneck on efficiently scaling up human traffic datasets. We propose a drone birdview image-based map (DBM) representation that requires minimal annotation and provides rich road context information. We evaluate multi-agent trajectory prediction using the DBM by incorporating it into a differentiable driving simulator as an image-texture-based differentiable rendering module. Our results demonstrate competitive multi-agent trajectory prediction performance when using our DBM representation as compared to models trained with rasterized HD maps.

1. Introduction

Creating realistic simulation environments is crucial for evaluating self-driving vehicles before they can be deployed in the real world. Recent studies have emphasized the use of learned models to generate more realistic driving behavior [17, 26, 33], which models imitate human-like driving by utilizing a probabilistic conditional model of multi-agent trajectories in a given environment. In such approaches, the quality of learned behavior is strongly dependent on the amount of data used for training [8, 11].

Typically, learning behavior models requires data consisting of the high-definition (HD) map for the given location and extracted agent tracks. While the latter can be extracted automatically from sensory data using modern computer vision algorithms with good accuracy [4, 8, 11], do-

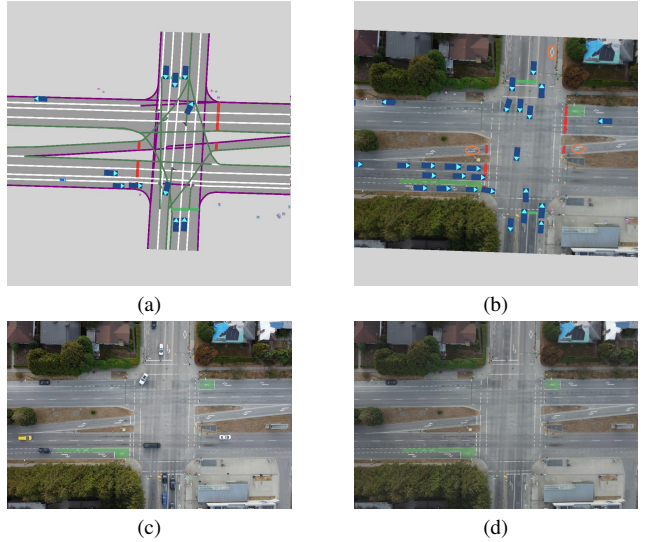


Figure 1. (a) An example of the simulating scene with the rasterized HD map representation compare to (b) the drone birdview map (DBM) representation rendered using our image-texture-based differentiable rendering module. DBM representation exhibits minimal annotations obtained from (c) the raw drone video recording frame with (d) agents removed and rich road context information highlighted by orange circles.

ing that for the former is still an open problem [7, 13, 32] and in practice, manual annotations are often used. Moreover, since it is important to ensure not only a large number of hours in the dataset but also a large variety of locations, manually annotating HD maps can become the most laborious part of creating a dataset. To make things worse, HD maps inevitably fail to capture important context, and increasing their detail like annotating sidewalks and crosswalks (see Fig. 2b) increases the cost of annotation. For example, the simplistic HD map scheme used in Fig. 1a does not reflect pedestrian crosswalks and bus lane designations.

In this study, we investigate the performance of behavioral models learned using aerial imagery instead of HD maps. Specifically, we record a dataset of human driv-

*¹Inverted AI, ²University of British Columbia, ³Mila

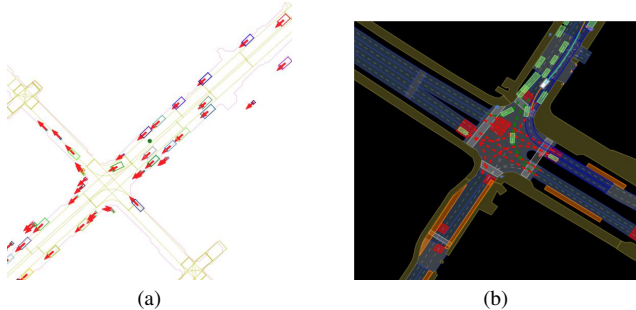


Figure 2. Examples of HD map from public motion planning datasets are shown in (a) Argoverse [5] and (b) NuPlan. The NuPlan map includes annotations like crosswalks and car park areas (shown in orange), which are not labeled in the Argoverse map.

ing behavior with a drone from a bird’s eye view, similarly to [28], and extract the background aerial image by averaging the collected video frames of the location. While other background extraction techniques can be applied [2, 14, 30], we find this simple averaging approach is sufficient for our use case. We refer to this image as the “drone birdview map” (DBM), emphasizing that it is both easy to obtain automatically and that it contains rich contextual information. Our primary motivation is to use such multi-agent behavioral models to construct realistic simulations, where DBM is assumed to be readily available at test time.

Learning driving models by behavioral cloning is known to suffer from the covariate shift, where prediction quality increases drastically with simulation time, and it has been demonstrated that this issue can be ameliorated by imitating in a differentiable simulator instead [24, 26, 33]. We use a similar approach, to incorporate the DBM into a differentiable simulator, we implement a custom differentiable renderer with Pytorch3D [20]. The renderer, illustrated in Fig. 3, uses DBM as background and places simple rasterizations of agents and traffic lights on top of it, as shown in Fig. 1b. To evaluate the impact of using DBM, we compare the original architecture of ITRA [33], which consumes rasterized views of HD maps shown in Fig. 1a, with the same model using DBM-based images shown in Fig. 1b. On widely used metrics minimum Average Displacement Error (minADE) and minimum Final Displacement Error (minFDE), ITRA trained with DBM representation outperforms ITRA trained using rasterized HD map representation. Utilizing a larger image feature encoder ResNet-18 [10], the ITRA model can achieve comparable metrics even on locations that were unseen during training.

2. Background

In this section, we will formally define our multi-agent trajectory prediction problem and give a brief overview of the multi-agent trajectory prediction model, ITRA, that we

use to evaluate our DBM representation. We will also introduce the concept of differentiable driving simulators applied in many trajectory prediction models including ITRA.

2.1. Multi-agent trajectory prediction

In this paper, we define the state for N agents across T time steps as s_T^N (following the notation used in [33]). For a specific agent i , its state $s_t^i = (x_t^i, y_t^i, \phi_t^i, v_t^i)$ for $t \in 1, \dots, T$ consists of the agent’s coordinates, as well as its direction and velocity relative to a stationary global reference frame. In the multi-agent trajectory prediction setting, we are interested in predicting the future joint state $s_{t_{obs}+1:T}^{1:N}$, given $s_{1:t_{obs}}^{1:N}$ observations while conditioning on the road context information. This information is traditionally represented by a so-called HD map. Such an HD map consists not only of road polygons, but separates lanes using lane boundaries (see Fig. 1a and Fig. 2a). HD maps generally also contain lane directions and can also include specific features such as crosswalks as shown Fig. 2b.

2.2. ITRA

We use ITRA [33] to investigate the validity of our primary claim. ITRA uses a conditional variational recurrent neural network (CVRNN) [6] model followed by a bicycle kinematic model [19] to jointly predict the next state of each agent in the scene. All interactions between the agents and the environment are encoded using differentially rendered birdview images. These birdview representations are centered at the agent of interest and rotated to match its orientation. Each agent i at timestep t is modeled as a CVRNN with recurrent state h_t^i and latent variables $z_t^i \sim \mathcal{N}(z_t^i, 0, \mathbf{I})$. After we obtain the corresponding ego birdview $b_t^i = \text{render}(i, s_{1:t}^{1:N})$ we produce the next action $a_t^i = f_\theta(b_t^i, z_t^i, h_{t-1}^i)$ where $h_t^i = f_\psi(h_{t-1}^i, b_t^i, a_t^i)$ is generated using a recurrent neural network. The action is then given to the bicycle kinematic model f_{kin} to generate the next state $s_{t+1}^i \sim \mathcal{N}(s_{t+1}^i; f_{kin}(s_t^i, a_t^i), \sigma \mathbf{I})$. The joint model $p(s_{1:T}^{1:N})$ factorizes as

$$\int \prod_{t=1}^T \prod_{i=1}^N p(s_{t+1}^i | s_t^i, a_t^i) p_\theta(a_t^i | b_t^i, z_t^i, h_{t-1}^i) p(z_t^i) dz_{1:T}^{1:N} da_{1:T}^{1:N}. \quad (1)$$

The model is trained jointly with a separate inference network $q_\phi(z_t^i | b_t^i, a_t^i, h_{t-1}^i)$ by maximizing the evidence lower bound (ELBO),

$$\sum_{t=1}^T \sum_{i=1}^N \mathbb{E}_{q_\phi(z_t^i | b_t^i, a_t^i, h_{t-1}^i)} [\log p_\theta(s_{t+1}^i | b_t^i, z_t^i, h_{t-1}^i)] - \text{KL} [q_\phi(z_t^i | b_t^i, a_t^i, h_{t-1}^i) || p(z_t^i)], \quad (2)$$

where

$$p_\theta(s_{t+1}^i | b_t^i, z_t^i, h_{t-1}^i) = p(s_{t+1}^i | s_t^i, a_t^i) p_\theta(a_t^i | b_t^i, z_t^i, h_{t-1}^i).$$

2.3. Differentiable driving simulators

Previous research has demonstrated that performing imitation learning within a differentiable simulator can help mitigate the distributional shift due to compounded error in open-loop behavior cloning methods [22, 24, 26]. These simulators typically consist of a differentiable kinematic model, such as the kinematic bicycle model, which produces the next state s_{t+1}^i given the current state and action pair. Additionally, they have a differentiable renderer that generates the ego-centered bird’s eye view image that includes the road context information and other agents in the scene. One of the main advantages of using such differentiable simulators is that the loss in Eq. (2) can be directly optimized using backpropagation as the state transition $p(s_{t+1}^i | s_t^i, a_t^i)$ is fully differentiable.

3. Related Work

Current methods to multi-agent modeling approach the problem by jointly predicting future trajectories using deep probabilistic models such as conditional variational auto-encoders (CVAEs) [12, 25–27, 33], normalizing flows [18, 21] and more recently diffusion models [31]. This family of multi-agent trajectory prediction models relies heavily on obtaining road context from HD maps, which requires manual annotations of lane center and boundary lines. To represent such HD maps, one approach is to render the semantic information of the map into a birdview image by employing different color schemes [24, 26, 33]. This image is then encoded using a convolutional neural network (CNN). Alternatively, recent work [9, 15] suggests representing road elements as a sequence of vectors that can be employed by a graph neural network which achieves better performance than the rendering approach. However, regardless of the embedding method, an annotated map has to be obtained, which our method bypasses completely. Moreover, the drone birdview image contains rich road context information such as left and right turn road marks and bicycle and bus lane markings without any annotation effort. In prior research [29], satellite image-based maps were used as a substitute for HD semantic maps, and the resulting findings indicated that trajectory prediction exhibited worse performance in such images. We point out that their satellite map representation does not contain traffic light information and the visual quality of the road context is limited. Our DBM representation contains traffic light states and agent states rendered by our differentiable rendering module with a higher visual quality of the road context information.

4. Proposed Method

Our method incorporates unlabelled drone RGB bird-view image into a simulation environment [33] using a differentiable renderer. We leverage image-texture-based ren-

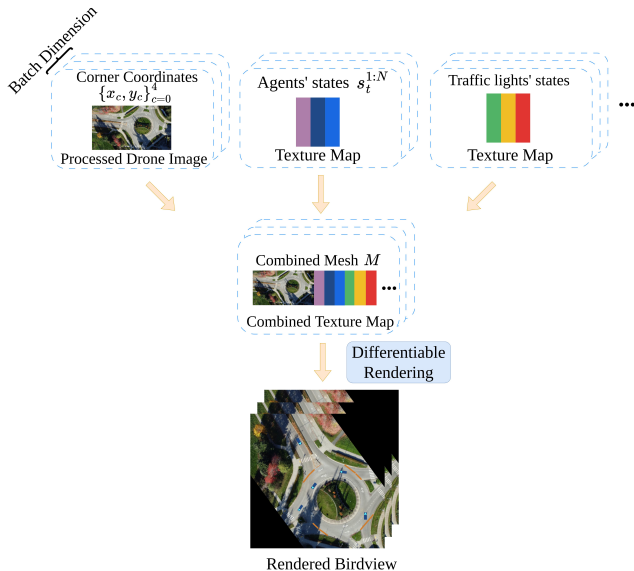


Figure 3. Image-texture-based Rendering Procedure

dering to represent the background of the simulated scene, as depicted in Fig. 1b. By embedding this rendering module into an existing end-to-end differentiable 2D driving simulator that targets multi-agent trajectory prediction, we can produce ego-rotated and egocentric birdview images b_t^i that utilize the proposed drone birdview map (DBM) background textures for multi-agent trajectory prediction models like ITRA. Furthermore, it provides a representation of the road context without information loss, as opposed to a rasterized birdview image from the labeled HD map shown in Fig. 1a. We introduce our image-texture-based differentiable rendering module in the following section.

4.1. Image-texture-based differentiable rendering.

Our image-textured-based rendering module is designed to be differentiable and efficient as it supports rendering in batch mode. The rendering process is illustrated in Fig. 3. Our module takes in the processed drone image of the recording location, along with its coordinates of the image corners $\{x_c, y_c\}$ for $c \in \{1 \dots 4\}$, the states of the agents $s_t^{1:N}$ at time t , and the traffic light states. We average the stabilized drone video frames to perform a simple yet effective background extraction of the video. This background extraction process serves to eliminate cars and other agents that may be present in the drone video. To differentiate agent types, each agent type is associated with a unique color in the texture map (see Fig. 3). The image corner coordinates are in the same global reference frame as the agent coordinates to align the map with the agents during rendering process. Using the aforementioned inputs, three distinct types of meshes are constructed, namely, the background mesh, agents mesh and the traffic light mesh along with

Method	Observation length					
	0.1 sec		0.5 sec		1 sec	
	minADE ₆ ↓	minFDE ₆ ↓	minADE ₆ ↓	minFDE ₆ ↓	minADE ₆ ↓	minFDE ₆ ↓
ITRA-HDM	0.88	1.79	0.63	1.35	0.50	1.04
ITRA-DBM	0.80	1.62	0.57	1.19	0.45	0.93
ITRA-ResNet18-DBM	0.85	1.76	0.63	1.40	0.50	1.10

Table 1. Validation set prediction errors on our in-house dataset. Compared to the ITRA-HDM, ITRA-DBM achieves an approximately 10% reduction in both average and final displacement errors across different observation lengths.

Method	Observation length					
	0.1 sec		0.5 sec		1 sec	
	Off-road rate↓	collision rate↓	Off-road rate↓	collision rate↓	Off-road rate↓	collision rate↓
ITRA-HDM	0.009	0.020	0.007	0.015	0.006	0.012
ITRA-DBM	0.012	0.018	0.010	0.015	0.008	0.012
ITRA-ResNet18-DBM	0.009	0.019	0.006	0.015	0.006	0.012

Table 2. Validation set infraction rate on our in-house dataset. The ITRA model trained with drone birdview maps achieves comparable performance to the ITRA model trained with rasterized HD maps in avoiding collisions. However, the former model exhibits slightly higher rates of off-road infractions. These findings indicate that switching to drone birdview representation introduces no effect on the model’s collision performance but may result in higher off-road infractions as drivable areas are not explicitly labeled.

their corresponding texture maps. These meshes are subsequently combined to form a concatenated mesh M with the combined texture map, which is then fed into a differentiable renderer, to render the simulating scene. Agents are rendered as bounding boxes with an additional triangle on top of each bounding box to indicate their direction. Traffic lights are rendered as rectangular bars at the stop line. The rendered birdview can be consumed by the trajectory prediction model as a representation of the environment for the ego agent which provides information about the road context and other agents in the scene.

5. Experiments

We evaluate ITRA with DBM (ITRA-DBM) on a dataset comprising 3.5 hours of traffic data collected using a commercial drone in 11 locations, primarily in Canada. These locations include roundabouts, signalized and unsignalized intersections, and highways, providing a diverse set of road geometries for training and evaluation. We have provided all of our training DBMs in Appx. 1.1 for reference. Besides testing on the training locations, we also test on two held-out locations to assess the generalization performance of the ITRA-DBM model. The first test location is close to the training DBM distribution, as it shares road geometry with the training maps. The second test location on the other hand, is markedly different in terms of road geometry, and the lane markings are more degraded. We additionally evaluate on a test aerial image from Bing aerial imagery [1] on one of the training locations (see Appx. 1.2). In total, we have 300k four-second long segments sampled at 10 Hz in our dataset of which 2.5% is used for testing. Our held-out test locations contain 1000 segments of four seconds each.

5.1. Implementation details

To compare ITRA-DBM with the original ITRA model that utilizes the rasterized HD map (ITRA-HDM), we apply the same training procedure on ITRA-DBM as our baseline, training each component of the network from scratch and using the same training hyper-parameters for ITRA-DBM and ITRA-HDM. We use an identical CNN encoder for encoding DBM which consists of a 4-layer CNN model for our ITRA-DBM model but also experiment with a ResNet-18 backbone to encode the DBM representation as it contains more information than rasterized HD map. To prevent our multi-agent trajectory model from depending too heavily on past observations [3], we train both of our models with a random observation length between 1 to 10 timesteps. We evaluate our models with different observation lengths, including a single observation, since in this case the predictions would mostly depend on the road features, highlighting any changes to the encoding thereof. We train both ITRA models for 14 epochs on 4 NVIDIA GeForce RTX 2080 Ti GPUs. The training time of ITRA-DBM is comparable to that of ITRA-HDM.

5.2. Evaluation Metrics

Two common evaluation metrics for evaluating trajectory prediction models are; ADE and FDE which measure how close the sampled trajectory is to the ground truth trajectory. In the multi-agent setting, ADE and FDE are averaged across all N agents. Typically, K trajectory predictions are taken and the generated trajectory with the minimum error is selected for calculating minADE_K and minFDE_K . As DBM does not explicitly label the drivable area, we would like to evaluate the prediction performance

		Observation length			
		0.1 sec		1 sec	
Test location	Method	minADE ₆ ↓	minFDE ₆ ↓	minADE ₆ ↓	minFDE ₆ ↓
1	ITRA-HDM	0.64	1.39	0.41	0.91
	ITRA-DBM	0.73	1.65	0.42	0.94
	ITRA-ResNet18-DBM	0.70	1.57	0.46	1.01
2	ITRA-HDM	0.72	1.54	0.48	1.03
	ITRA-DBM	0.77	1.78	0.57	1.28
	ITRA-ResNet18-DBM	0.70	1.53	0.50	1.10

Table 3. Test set prediction errors on held-out locations.

		Observation length			
		0.1 sec		1 sec	
Test location	Method	Off-road rate↓	Collision rate↓	Off-road rate↓	Collision rate↓
1	ITRA-HDM	0.002	0.013	0.000	0.009
	ITRA-DBM	0.003	0.008	0.001	0.004
	ITRA-ResNet18-DBM	0.003	0.020	0.001	0.005
2	ITRA-HDM	0.004	0.024	0.002	0.009
	ITRA-DBM	0.037	0.035	0.028	0.020
	ITRA-ResNet18-DBM	0.006	0.031	0.003	0.017

Table 4. Test set infraction rates on held-out locations.

of the ITRA-DBM model in terms of how often it commits off-road infractions. To accomplish this, we assume that we have access to a drivable surface mesh for evaluation purposes and we calculate the off-road rate using the method described in [16], where the off-road rate is zero when all four corners of the vehicle are within the drivable area. Furthermore, we also measure the collision rate in a multi-agent prediction setting using the intersection over union (IOU)-based collision metric from [16]. Both the off-road rate and collision rate reported in Tab. 2 and Tab. 4 are averaged across the number of agents, samples, and time.

5.3. Experimental results

We present results on the reserved final 2.5% of our drone recordings obtained at each location as our validation dataset, ensuring that the training data has no causal relationship to the test data. We jointly predict the trajectory for a time horizon of 40 time steps (4s) while observing the first 1, 5, or 10 time steps (0.1s, 0.5s or 1s) of the trajectory. Results on the validation dataset are presented in Tab. 1 and Tab. 2. ITRA-DBM performs competitively in reconstructing the ground truth trajectories across different observation lengths on the training map with validation segments. In terms of off-road rate, ITRA-DBM with a ResNet-18 backbone matches the performance of ITRA-HDM, while maintaining similar displacement errors compared to ITRA-HDM. Figure 4 shows validation examples of ITRA-HDM versus ITRA trained with the DBM representation.

On the two held-out locations (see Fig. 5), ITRA-HDM generalizes marginally better compared to ITRA-DBM (see Sec. 5, Tab. 4) of distance metrics. While it is expected that performance in generalization is better for HD maps

since the visual features are the same, these results show that for similar layouts the results are competitive. Since our DBM representation can be easily acquired for new locations without annotations, training on a larger and more diverse set of locations with a complete range of visual features will make these differences ultimately vanish. Furthermore, while the classic ITRA-DBM struggles with offroad infractions on held-out location 2, these results show that utilizing a more expressive image backbone helps to offset this performance gap, particularly on the off-road rate.

To further demonstrate the flexibility of our DBM representation, we acquired an aerial image from Bing aerial imagery of the same location as Fig. 4d to construct a larger DBM. Despite having different image conditions (such as shading and lighting) compared to the original training DBM, our trained ITRA-DBM achieves good prediction performance on this larger map with validation data segments as shown in the top row of Fig. 6. We also conduct an ablation experiment to investigate the effect of the road context information on our trajectory prediction model. Specifically, we tested the ITRA-DBM on a DBM where the road context information was removed and represented by a grey image, as shown in the bottom row of Fig. 6. Our results indicate that the performance of the ITRA-DBM significantly degrades under this condition, which supports our hypothesis that the road context information provided by our DBM plays a crucial role in our trajectory prediction model.

6. Conclusion

In this work, we address a critical bottleneck in scaling the dataset size for behavioral models used for simulating realistic driving. Specifically, the manual annota-

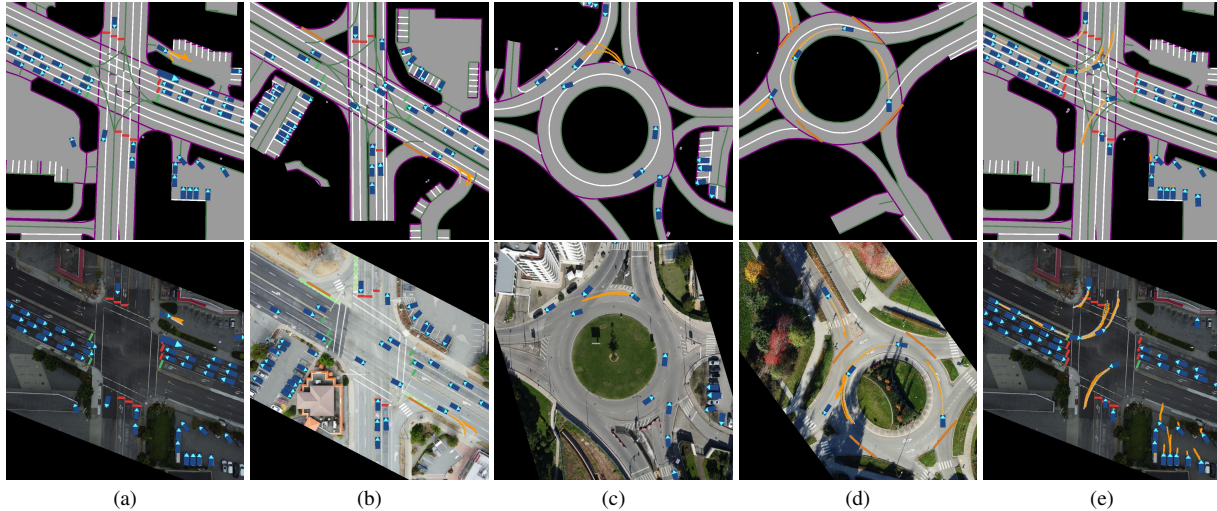


Figure 4. **Column (a-c)** Ego-only trajectory prediction of 40 timesteps based on the observation of only one initial timestep. We show 10 sampled trajectories in orange alongside the ground truth trajectory colored in grey for both ITRA-HDM and ITRA-DBM. Notice that ITRA trained with DBM representation generates more realistic samples by leveraging the rich road context, particularly in scenarios such as entering parking lots. **Column (d-e)** Examples of Multi-agent trajectory predictions on two different map representations.

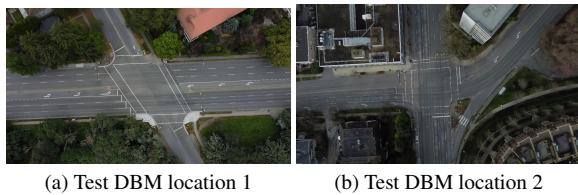


Figure 5. The two held-out locations used for testing.

tion of high-definition maps on new locations impedes the progress toward fully automated labeling of the dataset. Rather than pursuing the development of automated map labeling tools, which may introduce additional labeling noise, our proposed drone birdview image-based map (DBM) requires minimal annotations. By employing the DBM in an open-source driving simulator through our image-texture-based differentiable rendering, we illustrate that the DBM provides rich road context information for multi-agent trajectory prediction which resulted in more realistic samples. Our image-texture-based differentiable rendering module can be easily integrated into any existing behavioral prediction models that consumes bird’s eye view image as part of the agents’ state representation. This opens-up opportunities particularly in multi-agent behavior prediction domains that rely heavily on background context information such as pedestrian behavior predictions [23]. While our work has yielded promising results, there are still opportunities remaining for further improvement. These opportunities include an in-depth investigation of semantic or structure-based encoders for the DBM representation to improve on

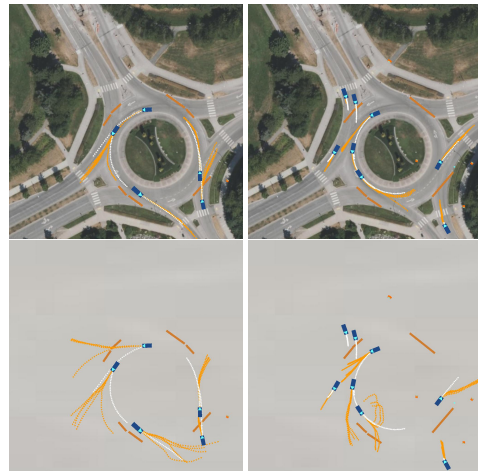


Figure 6. The top row shows the evaluation of ITRA-DBM on a Bing aerial image, while the bottom row shows the evaluation on an empty map. The white trajectories represent the ground truth trajectories obtained from validation segments at the same location, and the orange trajectories display 5 sampled trajectories of the ITRA-DBM model. Our ITRA-DBM model predicts road context-aware trajectories on this aerial image which has different lighting and shading conditions compare to the training DBM. As an ablation, When no road context information is provided, the performance of ITRA-DBM degrades significantly.

the off-road metrics. Finally, while we constructed DBMs from drone recordings, they could also be employed when collecting data from the vehicle by utilizing existing aerial imagery, although additional effort would be required to align such images to the extracted agent tracks.

References

- [1] Bing Maps. Website. Accessed: April 12, 2023. 4
- [2] Olivier Barnich and Marc Van Droogenbroeck. Vibe: A universal background subtraction algorithm for video sequences. *IEEE Transactions on Image processing*, 20(6):1709–1724, 2010. 2
- [3] Hédi Ben-Younes, Eloi Zablocki, Mickaël Chen, Patrick Pérez, and Matthieu Cord. Raising context awareness in motion forecasting. In *Proceedings of the IEEE/CVF Conference on Computer Vision and Pattern Recognition*, pages 4409–4418, 2022. 4
- [4] Holger Caesar, Juraj Kabzan, Kok Seang Tan, Whye Kit Fong, Eric Wolff, Alex Lang, Luke Fletcher, Oscar Beijbom, and Sammy Omari. nuplan: A closed-loop ml-based planning benchmark for autonomous vehicles. *arXiv preprint arXiv:2106.11810*, 2021. 1
- [5] Ming-Fang Chang, John W Lambert, Patsorn Sangkloy, Jagjeet Singh, Slawomir Bak, Andrew Hartnett, De Wang, Peter Carr, Simon Lucey, Deva Ramanan, and James Hays. Argoverse: 3d tracking and forecasting with rich maps. In *Conference on Computer Vision and Pattern Recognition (CVPR)*, 2019. 2
- [6] Junyoung Chung, Kyle Kastner, Laurent Dinh, Kratarth Goel, Aaron C Courville, and Yoshua Bengio. A recurrent latent variable model for sequential data. 2015. 2
- [7] Mahdi Elhousni, Yecheng Lyu, Ziming Zhang, and Xinming Huang. Automatic building and labeling of hd maps with deep learning. In *Proceedings of the AAAI Conference on Artificial Intelligence*, volume 34, pages 13255–13260, 2020. 1
- [8] Scott Ettinger, Shuyang Cheng, Benjamin Caine, Chenxi Liu, Hang Zhao, Sabeek Pradhan, Yuning Chai, Ben Sapp, Charles R Qi, Yin Zhou, et al. Large scale interactive motion forecasting for autonomous driving: The waymo open motion dataset. In *Proceedings of the IEEE/CVF International Conference on Computer Vision*, pages 9710–9719, 2021. 1
- [9] Jiyang Gao, Chen Sun, Hang Zhao, Yi Shen, Dragomir Anguelov, Congcong Li, and Cordelia Schmid. Vectornet: Encoding hd maps and agent dynamics from vectorized representation. In *Proceedings of the IEEE/CVF Conference on Computer Vision and Pattern Recognition (CVPR)*, June 2020. 3
- [10] Kaiming He, Xiangyu Zhang, Shaoqing Ren, and Jian Sun. Deep residual learning for image recognition. In *Proceedings of the IEEE conference on computer vision and pattern recognition*, pages 770–778, 2016. 2
- [11] John Houston, Guido Zuidhof, Luca Bergamini, Yawei Ye, Long Chen, Ashesh Jain, Sammy Omari, Vladimir Iglovikov, and Peter Ondruska. One thousand and one hours: Self-driving motion prediction dataset. In *Conference on Robot Learning*. PMLR, 2021. 1
- [12] Namhoon Lee, Wongun Choi, Paul Vernaza, Christopher Bongsoo Choy, Philip H. S. Torr, and Manmohan Chandraker. Desire: Distant future prediction in dynamic scenes with interacting agents. In *CVPR*, 2017. 3
- [13] Qi Li, Yue Wang, Yilun Wang, and Hang Zhao. Hdmapnet: An online hd map construction and evaluation framework. *2022 International Conference on Robotics and Automation (ICRA)*, pages 4628–4634, 2021. 1
- [14] Xiyang Li, Guoming Li, Qiuxiao Huang, Zhenbo Wang, and Zhi Yu. An adaptive background extraction method in traffic scenes. *Optik*, 156:659–671, 2018. 2
- [15] Ming Liang, Bin Yang, Rui Hu, Yun Chen, Renjie Liao, Song Feng, and Raquel Urtasun. Learning lane graph representations for motion forecasting. In *Computer Vision—ECCV 2020: 16th European Conference, Glasgow, UK, August 23–28, 2020, Proceedings, Part II 16*, pages 541–556. Springer, 2020. 3
- [16] Vasileios Lioutas, Adam Ścibior, and Frank Wood. TITRATED: Learned Human Driving Behavior without In-fractions via Amortized Inference. 2021. 5
- [17] Yunpeng Liu, Jonathan Wilder Lavington, Adam Scibior, and Frank Wood. Vehicle type specific waypoint generation. In *IROS*, pages 12225–12230. IEEE, 2022. 1
- [18] Xiaobai Ma, Jayesh K Gupta, and Mykel J Kochenderfer. Normalizing flow policies for multi-agent systems. In *Decision and Game Theory for Security: 11th International Conference, GameSec 2020, College Park, MD, USA, October 28–30, 2020, Proceedings 11*, pages 277–296. Springer, 2020. 3
- [19] Philip Polack, Florent Alché, Brigitte d’Andréa Novel, and Arnaud de La Fortelle. The kinematic bicycle model: A consistent model for planning feasible trajectories for autonomous vehicles? In *IEEE Intelligent Vehicles Symposium (IV)*, 2017. 2
- [20] Nikhila Ravi, Jeremy Reizenstein, David Novotny, Taylor Gordon, Wan-Yen Lo, Justin Johnson, and Georgia Gkioxari. Accelerating 3d deep learning with pytorch3d. *arXiv:2007.08501*, 2020. 2
- [21] Nicholas Rhinehart, Rowan McAllister, Kris Kitani, and Sergey Levine. Precog: Prediction conditioned on goals in visual multi-agent settings. In *Proceedings of the IEEE/CVF International Conference on Computer Vision (ICCV)*, October 2019. 3
- [22] Stéphane Ross, Geoffrey Gordon, and Drew Bagnell. A reduction of imitation learning and structured prediction to no-regret online learning. In *Proceedings of the fourteenth international conference on artificial intelligence and statistics*, pages 627–635. JMLR Workshop and Conference Proceedings, 2011. 3
- [23] Amir Sadeghian, Vineet Kosaraju, Ali Sadeghian, Noriaki Hirose, Hamid Rezafofighi, and Silvio Savarese. Sophie: An attentive gan for predicting paths compliant to social and physical constraints. In *Proceedings of the IEEE/CVF conference on computer vision and pattern recognition*, pages 1349–1358, 2019. 6
- [24] Oliver Scheel, Luca Bergamini, Maciej Wolczyk, Błażej Osiański, and Peter Ondruska. Urban driver: Learning to drive from real-world demonstrations using policy gradients. In *Conference on Robot Learning*, pages 718–728. PMLR, 2022. 2, 3
- [25] NN Sriram, Buyu Liu, Francesco Pittaluga, and Manmohan Chandraker. Smart: Simultaneous multi-agent recurrent trajectory prediction. In *Computer Vision—ECCV 2020: 16th*

European Conference, Glasgow, UK, August 23–28, 2020, Proceedings, Part XXVII 16, pages 463–479. Springer, 2020. [3](#)

- [26] Simon Suo, Sebastian Regalado, Sergio Casas, and Raquel Urtasun. TrafficSim: Learning to simulate realistic multi-agent behaviors. In *CVPR*, 2021. [1](#), [2](#), [3](#)
- [27] Yichuan Tang and Ruslan Salakhutdinov. Multiple futures prediction. In *NeurIPS*, 2019. [3](#)
- [28] Wei Zhan, Liting Sun, Di Wang, Haojie Shi, Aubrey Clause, Maximilian Naumann, Julius Kümmerle, Hendrik Königshof, Christoph Stiller, Arnaud de La Fortelle, and Masayoshi Tomizuka. INTERACTION Dataset: An International, Adversarial and Cooperative moTION Dataset in Interactive Driving Scenarios with Semantic Maps. *arXiv preprint arXiv:1910.03088*, 2019. [2](#)
- [29] Kunpeng Zhang, Xiaoliang Feng, Lan Wu, and Zhengbing He. Trajectory prediction for autonomous driving using spatial-temporal graph attention transformer. *IEEE Transactions on Intelligent Transportation Systems*, 2022. [3](#)
- [30] Rui Zhang, Weiguo Gong, Andrew Yaworski, and Michael Greenspan. Nonparametric on-line background generation for surveillance video. In *Proceedings of the 21st International Conference on Pattern Recognition (ICPR2012)*, pages 1177–1180. IEEE, 2012. [2](#)
- [31] Ziyuan Zhong, Davis Rempe, Danfei Xu, Yuxiao Chen, Sushant Veer, Tong Che, Baishakhi Ray, and Marco Pavone. Guided conditional diffusion for controllable traffic simulation. *arXiv preprint arXiv:2210.17366*, 2022. [3](#)
- [32] Yiyang Zhou, Yuichi Takeda, Masayoshi Tomizuka, and Wei Zhan. Automatic construction of lane-level hd maps for urban scenes. In *2021 IEEE/RSJ International Conference on Intelligent Robots and Systems (IROS)*, pages 6649–6656, 2021. [1](#)
- [33] Adam Ścibior, Vasileios Lioutas, Daniele Reda, Peyman Bateni, and Frank Wood. Imagining the road ahead: Multi-agent trajectory prediction via differentiable simulation. In *ITSC*, 2021. [1](#), [2](#), [3](#)

7. Appendix

7.1. Drone birdview training maps



7.2. The Bing aerial image

